We are IntechOpen, the world's leading publisher of Open Access books
Built by scientists, for scientists

6,900
Open access books available

186,000
International authors and editors

200M
Downloads

154
Countries delivered to

Our authors are among the

TOP 1%
most cited scientists

12.2%
Contributors from top 500 universities

CLARIVATE ANALYTICS
BOOK CITATION INDEX
INDEXED

WEB OF SCIENCE™

Selection of our books indexed in the Book Citation Index
in Web of Science™ Core Collection (BKCI)

Interested in publishing with us?
Contact book.department@intechopen.com

Numbers displayed above are based on latest data collected.
For more information visit www.intechopen.com

Numerical Simulation of Fluid Flow and Hydrodynamic Analysis in Commonly Used Biomedical Devices in Biofilm Studies

Mohammad Mehdi Salek and Robert John Martinuzzi
University of Calgary
Canada

1. Introduction

Biofilms are microbial communities which can form on most biotic or abiotic surfaces including glass, metal, plastic, rocks, and live tissues. These colonies begin with individual planktonic bacterial cells that attach to a surface and then start to generate a sticky Extracellular Polymeric Substance (EPS). This complex polysaccharide matrix contributes to a modification of the phenotypic status of bacteria and protects them against the detrimental changes in the microenvironment surrounding the biofilms. These phenotypic changes typically confer increased resistance to antibiotics or to the host defence system in patients. This enhanced tolerance is associated with significant problems, such as hospital acquired infections, equipment damage, and energy losses (Trachoo, 2003; Percival et al., 2004), making biofilms a major concern in different industries.

In health care, biofilms are responsible for 65% of hospital acquired infections, adding more than $1 billion annually for treatment costs in United States (Percival et al., 2004). Hospital acquired infections are the fourth leading cause of death in the U.S. accounting for 2 million death annually (Wenzel, 2007). Almost all types of biomedical devices and tissue engineering constructs are susceptible to biofilm formation (Bryers & Ratner, 2004; Bryers, 2008). Biofilms are particularly associated with a variety of bloodstream infections related to indwelling medical devices (e.g. urinary and cardiovascular catheters, vascular and ocular prostheses, prosthetic heart valves, cardiac pacemakers, cerebrospinal fluid shunts and other types of surgical devices). They are also responsible for chronic infections and recalcitrant diseases such as cystic fibrosis and periodontal diseases (Castelli et al.,2006; MacLeod et al., 2007; Meda et al., 2007; Presterl et al., 2007; Murray et al., 2007; Bryers, 2008; Phillips et al., 2008).

In industrial applications, biofilms can clog filters, block pipes and induce corrosion. They are responsible for billions of dollars yearly in equipment damage, energy losses, and water system contamination (Geesey & Bryers 2000). Additional costs associated with biofilm contaminations include disinfection, preventive maintenance, mitigation and replacement of contaminated materials.
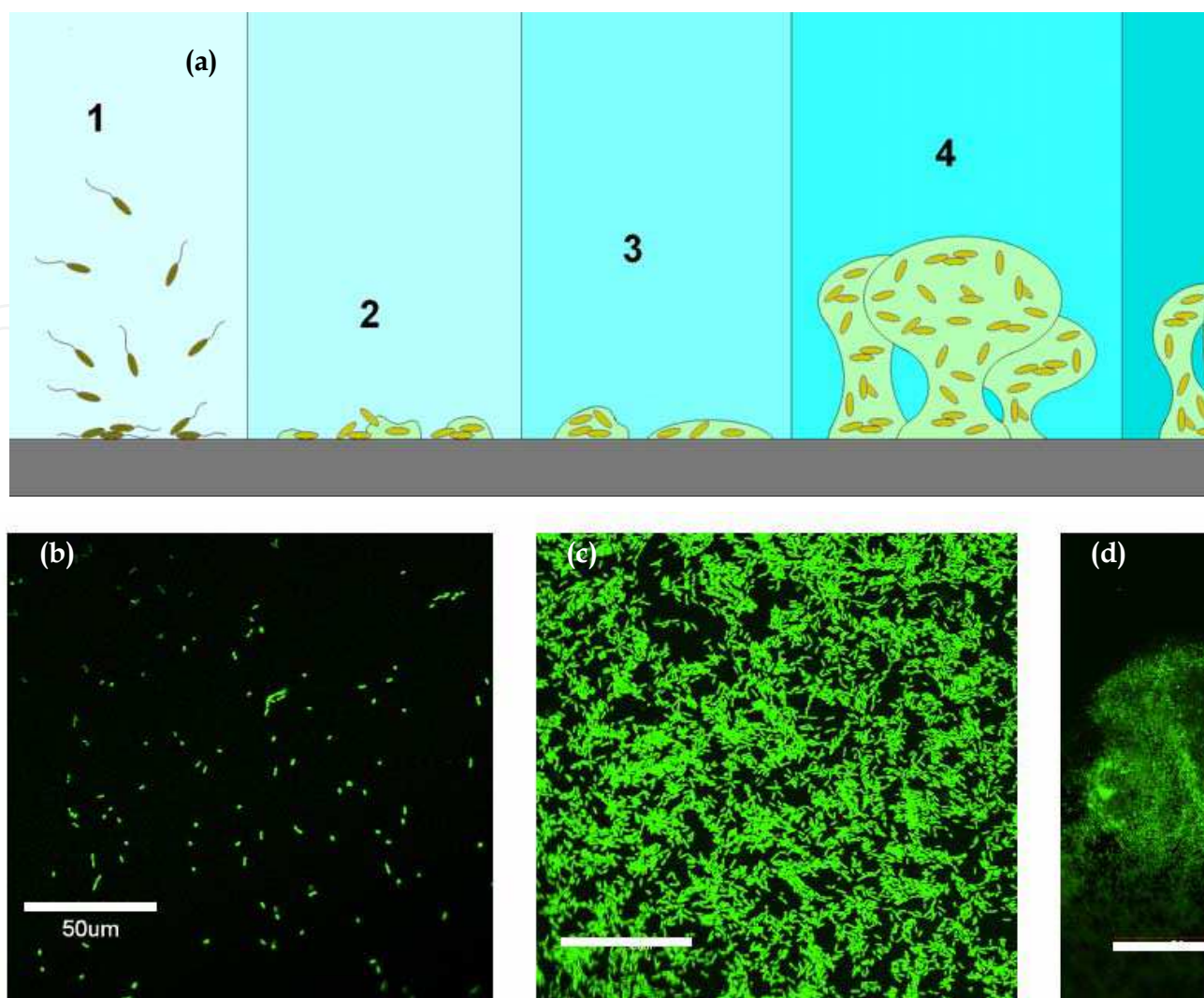
Fig. 1. a) Biofilm development process; b) Representative Confocal Scanning Laser Microscopy (
aeruginosa O1 biofilms corresponding to step 1 and 2; c) corresponding to step 3; d) Seeding disp
to step 5 (Salek et al., 2009). All bars are 50 μm

Biofilm formation and behaviour is a result of several generally coupled physical, chemical and biological processes as illustrated in Fig. 1:

1. Transport of bacterial cells from the bulk liquid to the surfaces and then adhesion to the wall. The process of attachment is either reversible or irreversible. If the adhesion is reversible, the bacterial cells can still be detached by small shear forces or their own motility (Marshal, 1985).
2. After the attachment, bacterial cells start to produce EPS. This polymeric matrix acts like glue holding the biofilms together.
3. The next step is surface colonization and biofilm growth through a combination of cell division, cellular growth, EPS production and attachment/sequestering of new cells.
4. Biofilms develop to form morphologically more complex structures.
5. The final stage of biofilm formation is dissemination and recolonization. There are two important mechanisms here:
   i. Biofilm detachment due to nutrient depletion and hydrodynamic forces. It occurs when external forces through the shear stress are larger than the internal strength of the micro-colonies (Horn et al., 2003).
   ii. Seeding dispersal in which single cells may be released from the colony

All these stages are influenced by transport processes and thus the interaction with the fluid environment. While the fluid (e.g. blood, water or oil) is a source of nutrients, it also governs the transport of signaling molecules or of the bacteria and can provide the mechanical stimulus for regulating gene expression. Hence, the hydrodynamics of the fluid over biofilms is one of the more important factors affecting biofilm formation, structure and activity (Christensen, 1989; Stoodley et al., 1999; Purevdorj et al., 2002; Manz et al., 2003; Chen, 2005; Gjersing et al., 2005; Salek et al., 2009). The flow field affects each process of biofilm formation by changing the substrate concentration around the colonies, which influences the transport of bacteria and nutrients, and regulates the physiological properties of these complex structures by changing the mechanical shear stresses at the fluid-biofilm interface.

A broad range of techniques and models have been developed for in-vitro studies of the biofilm behavior under different environmental conditions. Among these, different types of tube flow cells are widely used to manipulate the hydrodynamics of flow around the biofilms (Manz et al., 2003; Gjersing et al., 2005). Tube flow cells and parallel plate flow chambers are commonly used in biofilm and microbiology studies to manipulate the hydrodynamics of flow surrounding the biofilms. Tube flow cells can be incorporated into different flow systems working over a wide range of flow regime from laminar to turbulent, and therefore they can be easily used to study the influence of flow velocity on biofilms structure and behavior (Stoodley et al., 2001b). Hosoi et al. (1986) investigated the effects of fluid velocity and shear on the biofilm formation in round pipes and found that an optimum shear to maximize the biofilm accumulation existed. Manz et al. (2003) imaged the velocity distribution over the biofilms in round tubes and showed that the local shear stress calculated from the measured velocity profiles at the biofilm interface was higher than the average wall shear stress calculated on the base of the mean flow velocity. This coupling between the stress field and biofilm growth illustrates the need for a detailed knowledge of the near-wall flow even in for the apparently simple round tube flow cell.

Albeit round tubes provide simpler hydrodynamic conditions, square or rectangular flow cells are often preferred for experiments to provide optical or microelectrode access (Gjersing et al., 2005). Stoodley et al. (2001a), for example, used square tubes to study biofilm properties under different fluid shear and environment conditions. They found that the hydrodynamic shear and local ionic environment influenced biofilm structure, cohesive
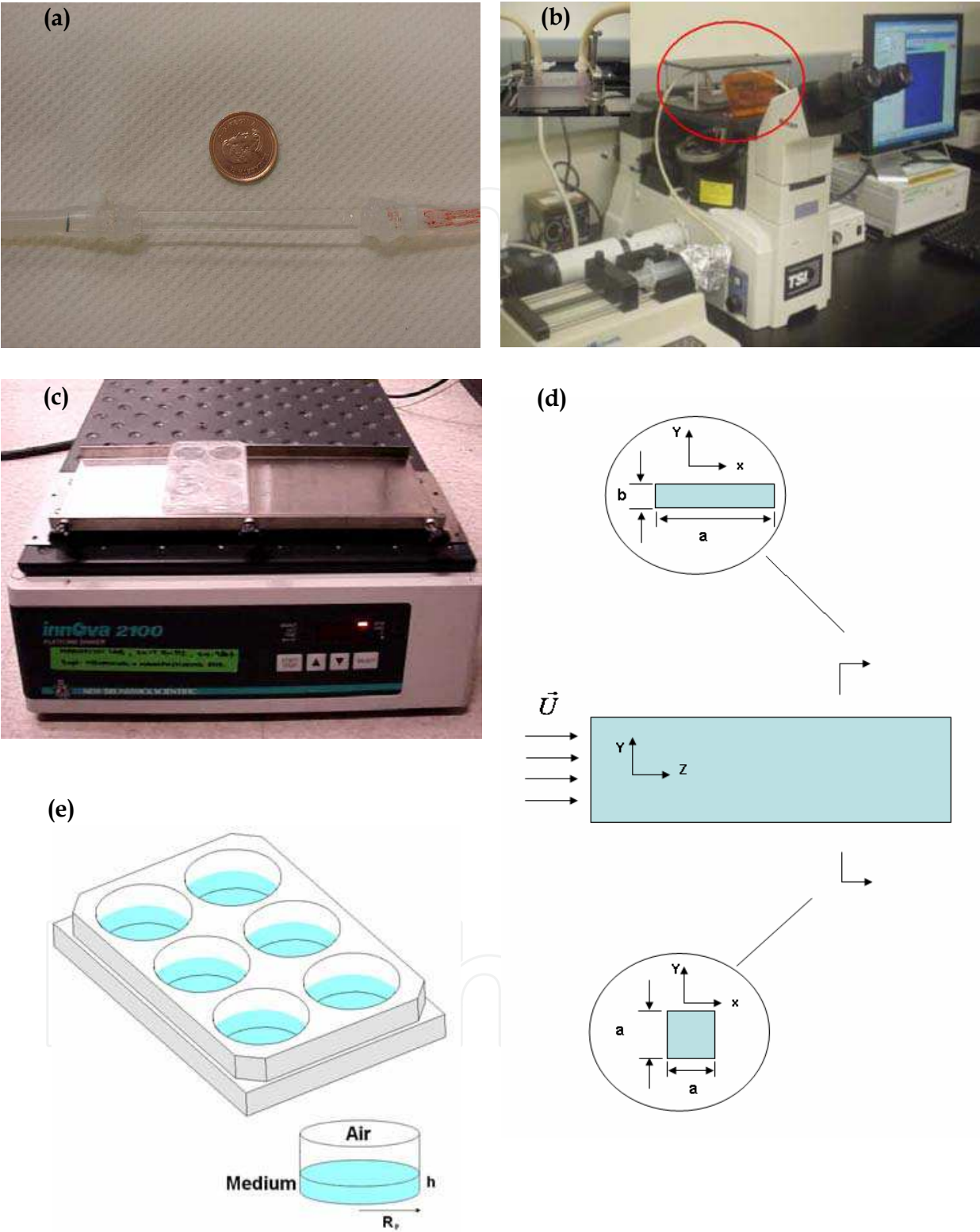
Fig. 2. Biomedical devices used in biofilm studies, Biofilm Engineering Research Group, University of Calgary (a) Glass tube flow cell; (b) Micro parallel-plate chamber located on a micro-PIV system; (c) 6-well plate mounted on an orbital shaker; (d) Schematic of rectangular and square flow cells; (e) Schematic of the 6-well plate

strength and material properties. Ebrahimi et al., (2005) showed that substrate limitation can reduce growth in the corners of rectangular channels. Gjersing et al. (2005) employed magnetic resonance microscopy to characterize the advective transport through a square duct geometry with biofilms covering the circumference. They observed that the presence of secondary flows can alter the mass transport in the reactor. Salek et al. (2009) studied the effects of non-uniform local hydrodynamic conditions arising in square and rectangular glass flow cells on PAO1 biofilm formation and structure. Their study showed that even under nominally uniform flow conditions, the spanwise changes in the hydrodynamic parameters can effectively change the biofilm colonization, structure and antimicrobial response.

Whereas flow cells are well suited for controlling hydrodynamic conditions, their use is generally impractical when many concurrent microbial tests over a range of flow conditions are required. High-throughput devices, commonly used to study microbial biofilms (Sillankorva et al., 2008; Sousa et al., 2008), are very practical when many parallel tests are needed in a short time period. They are widely used for rapid testing of antibiotic susceptibility and conducting many replicates. But the hydrodynamics inside these devices is not well understood. Therefore, they have been rarely used to study the biofilms under controlled hydrodynamic conditions.

The main purpose of the present work is to develop and apply different computational techniques to simulate and analyse the flow field and local hydrodynamics over the biofilm culture area in different biomedical devices as are typically used in biofilm studies (Fig. 2). In the first part, the influence of the flow cell geometry on the hydrodynamics and mass transport acting locally on biofilms is investigated computationally for different types of flow cells. In the second part of this chapter, the unsteady oscillating flow arising in high-throughput devices is investigated. To this end a numerical simulation of the flow in an agitated well plate and MBEC™ device, commonly used high-throughput devices for biofilm studies, is presented.

2. Hydrodynamic characteristics of tube flow cells and parallel plate flow chambers

Results obtained in flow cells used in different microbiology studies are sometimes contradictory. It is thus hypothesized that the differences in the biofilms responses can be directly related to the hydrodynamic changes caused by the flow cell geometry (Salek & Martinuzzi, 2007; Salek et al., 2009). In this part, the shear stress and mass transport, the most important parameters in biofilm studies, are investigated in different types of flow cells. The effects of flow cell configuration, flow velocity and substrate diffusivity on shear stress and mass distribution are presented.

2.1 Numerical method and study parameters
The coupled three-dimensional (3D) steady-state Navier-Stokes and continuity equations for incompressible flow

$$\rho(\vec{v} \cdot \nabla)\vec{v} = -\nabla p + \mu \nabla^2 \vec{v} \tag{1}$$

$$\nabla \cdot \vec{v} = 0 \tag{2}$$

were solved where $\vec{v}$, μ, ρ and p are velocity, dynamic viscosity, density and pressure respectively.

At the inlet, a uniform axial velocity was assumed, corresponding to the average bulk velocity:

$$U_m = \frac{Q}{A} \tag{3}$$

where A is the cross sectional flow areal and Q is the total volumetric flow rate. This inlet condition is a reasonable assumption when the length of tubes is sufficient to allow fully developed flow. At the outlet, a fully developed flow condition (zero velocity gradients in the axial direction) was imposed. A no slip boundary condition was imposed at the walls. This boundary condition implies a zero-velocity at the walls (for a clean flow cell). For further details please refer to (Salek & Martinuzzi, 2007) and (Salek et al., 2009).

The configuration of any physical system can be described as a function of relevant system parameters such as forces, fluxes and geometry, which are characterized in terms of non-dimensional numbers.

The non-dimensional form of shear stress can be defined in terms of Darcy-Weisbach friction factor and Reynolds number (Spiga et al., 1994; Salek et al., 2009):

$$\bar{\tau} = \frac{\tau_w}{\mu U_m / 8D_h} = f \cdot \mathrm{Re}_D \tag{4}$$

Where the friction factor, f, and Reynolds number, Re_D, are:

$$f = \frac{8\tau_w}{\rho U_m^2} \tag{5}$$

$$\mathrm{Re}_D = \frac{\rho U_m D_h}{\mu} \tag{6}$$

in which τ_w is the wall shear stress. D_h is the hydraulic diameter :

$$D_h = \frac{4A}{\Gamma} \tag{7}$$

where Γ denotes the wetted perimeter of the tube.

The friction factor is given by:

$$f = \frac{K}{\mathrm{Re}_D} \tag{8}$$

where K is a constant depending only on the tube geometry. For laminar flow, K = 64 in round tubes. In rectangular tubes, K is calculated according to the following equation [Tsanis et al., 1982; Leutheusser, 1984]:

$$K = \left(96\alpha^2 / (\alpha+1)^2\right)\left(1 - \left((192/\pi^5\alpha)\right)\right)$$
$$(\tanh(3\pi\alpha/2) + 3^{-5}\tanh(3\pi\alpha/2) + ...))^{-1} \tag{9}$$

in which $\alpha = a/b$ is the aspect ratio of the channel of width a and height b. In parallel plate flow chambers, the two-dimensional limit K = 96 is approached as $\alpha \gg 1$.

Numerical Simulation of Fluid Flow and Hydrodynamic Analysis
in Commonly Used Biomedical Devices in Biofilm Studies
199

In previous biofilm studies in either laminar or turbulent regimes (Cao and Alaerts 1995; Stoodley et al. 2001a,b; Dunsmore et al. 2002), the wall shear stress and friction factor for a rectangular channel were approximated (as an average) based on the round tube results. In laminar flow, the average shear stress at the wall is estimated as:

$$\tau_{wD} = \frac{8\mu U_m}{D_h} \qquad (10)$$

However, the latter equation is erroneously used for typical geometric configurations of small aspect ratio. For example, for a square cross-section flow cell ($\alpha = 1$) and a two-dimensional high aspect ratio flow cell ($\alpha = \infty$), K =56 and K=96 respectively. This leads to 70% changes in the average wall shear stress under nominally uniform flow conditions (i.e. the same bulk velocity and hydraulic diameter). Different flow cells with different geometric configurations are compared in (Salek et al., 2009).

Although the analyses mentioned above are done for a clean reactor, they can be used for early biofilm formation (i.e. thin layer with a relatively simple structure). From a fluid mechanics point-of-view, the adhered bacterial cells and small micro-colonies can be viewed as small surface roughness elements, or protrusions, embedded deeply in the low momentum wall layer. Under these conditions, Miksis and Davies (1994) have shown that the macroscopic wall shear stress can be approximated by the no slip boundary condition at the average roughness height, and therefore the flow prediction in a clean reactor can be a good guide in the study of early stages of biofilm formation (Salek et al., 2009). For older biofilms with morphologically complex structures an effective slip condition should be defined at the solid boundaries (Miksis & Davies, 1994). Moreover, if the roughness is
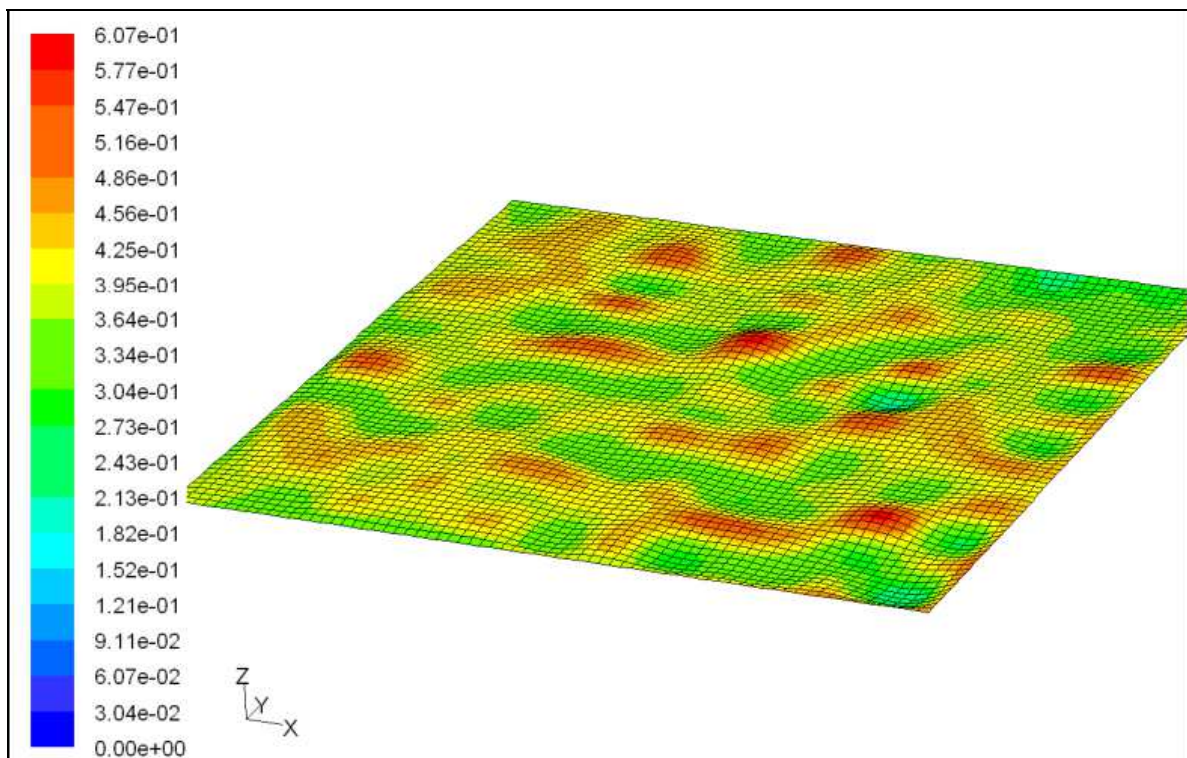

Fig. 3. Wall shear stress distribution over the reconstructed Endothelial Cells in a μ-channel as determined by CFD (unit is in Pa). Reprinted from (Dol et al., 2010), ASME. Note that shear stress distribution correlates well with local roughness height

comparable to the height of flow cell, the actual surface should be modeled (e.g. endothelial cell cultures in micro-flow chambers, shown schematically in figure 3, from (Dol et al., 2010). This figure shows that when the roughness height is not negligible within the flow cell, the surface shear stress distribution can not be adequately represented by a global average.

In spite of the fact that biofilm formation is a dynamic process of growth and detachment, models under steady conditions can provide useful insights on the effects of flow cell configuration on substrate concentration distribution (Salek & Martinuzzi, 2007). To this end, the substrate concentration was numerically simulated inside the flow cells by solving the mass transport equation (Salek & Martinuzzi, 2007):

$$\vec{v} \cdot \nabla C = D \nabla^2 C \tag{11}$$

where C and D are the substrate concentration and diffusivity, respectively. Oxygen was assumed as the substrate and a uniform distribution of biofilms (consuming the oxygen from the medium) was assumed on the walls. A uniform concentration of oxygen (C_{in}) at the inlet and no streamwise gradient of mass ($\partial C / \partial z = 0$) at the outlet were assumed as the mass boundary conditions here. The consumption of oxygen by biofilms was assumed to follow the Monod kinetics (Picioreanu et al., 2000; Rittmann et al., 2001). The microbial activities within the biofilms consume the substrate from the bulk flow, and then create a substrate flux from the bulk liquid to the biofilms at the walls. This substrate flux is a function of substrate concentration right at the top of the biofilm surfaces and was set at the walls:

$$D \frac{\partial C(x,0,z)}{\partial y} = \eta \hat{q}_{max} X_f L_f \frac{C(x,0,z)}{K_s + C(x,0,z)} \tag{12}$$

$$D \frac{\partial C(x,b,z)}{\partial y} = \eta \hat{q}_{max} X_f L_f \frac{C(x,b,z)}{K_s + C(x,b,z)} \tag{13}$$

$$D \frac{\partial C(0,y,z)}{\partial x} = \eta \hat{q}_{max} X_f L_f \frac{C(0,y,z)}{K_s + C(0,y,z)} \tag{14}$$

$$D \frac{\partial C(a,y,z)}{\partial x} = \eta \hat{q}_{max} X_f L_f \frac{C(a,y,z)}{K_s + C(a,y,z)} \tag{15}$$

K_s, $\hat{q}_{max}$, X_f, L_f, and η are the half maximum rate concentration, maximum specific rate of substrate utilization, biofilm density, biofilm thickness, and effectiveness factor respectively. In fact, η is the ratio of the real flux to the flux occurring when the biofilm is fully penetrated at the top surface concentration. The effectiveness factor shows the effect of internal mass transport resistance. In our study, the biofilms were idealized with uniform thickness and density (Rittmann et al., 2001). Oxygen was modeled as a continuum species in a bulk flow.

The governing equations were solved using the Computational Fluid Dynamics (CFD) code FLUENT 6.2. Distributions of substrate concentration were solved with a species transport model. An external C++ user defined function (UDF) linked to FLUENT was used to define

and discretize the mass boundary condition at the wall. This was done by defining the mass flux using the values of mass concentration on the wall face and in the adjacent cell, and then overwriting the value of concentration on the face according to the concentration of the adjacent cell and desired flux.

The non-dimensional substrate concentration is defined as:

$$\overline{C} = \frac{C}{C_{in}} \tag{16}$$

And the mass Peclet number, which measures the ratio of convective to diffusive mass flux, is defined as:

$$Pe = \frac{U_m D_h}{D} \tag{18}$$

The other important non-dimensional parameter in mass transfer is the Damkohler number (Tilles et al., 2001; Zeng et al., 2006):

$$Da = \frac{\eta X_f q_{max} L_f D_h}{C_{in} D} \tag{19}$$

Da is the ratio of substrate reaction rate at the wall to substrate diffusion from the medium. Biofilms with higher activity present higher *Da*. Damkohler was kept constant at 0.5 in our study. K_s was assumed constant except in the model verification section, where it was set to zero to simplify the boundary condition.

2.2 Model verification

The area weighted average of the wall shear stress in the fully developed regions in each flow cells was compared with the values obtained by the shear equation considering the geometry configuration. The results were in good agreement (not shown here). The mass transport model used in this study was verified through the comparison of the analytical solution for oxygen transport with the results gained at the bottom of a two-dimensional (2D) flow cell. No flux at one wall and a constant substrate flux at the other wall were assumed. The flow velocity was constant and uniform through the flow cell. To simplify the boundary condition just in model verification, we put $K_s = 0$ which means that the substrate flux is constant at the maximum value. The analytical solution for the oxygen concentration along the bottom wall is obtained by the following equation (Carslaw et al., 1959; Tilles et al., 2001):

$$\begin{aligned} C / C_{in} = 1 &- z \frac{l}{bU_m} \frac{\eta X_f q_{max} L_f}{C_{in}} - \frac{\eta X_f q_{max} L_f b}{3 C_{in} D} \\ &+ \frac{2}{\pi^2} \frac{\eta X_f q_{max} L_f b}{C_{in} D} \sum_{n=1}^{\infty} \frac{(-1)^n}{n^2} \cos(n\pi) \exp[-\frac{D l \pi^2 n^2 z}{U_m b^2}] \end{aligned} \tag{20}$$

Figure 4 compares the calculated mass distribution at the base with the analytical solution showing a good agreement. As will be discussed later, at lower mass Peclet number less

substrate is provided by the biofilms and nutrient depletion can happen through the flow cell ($C \approx 0$).
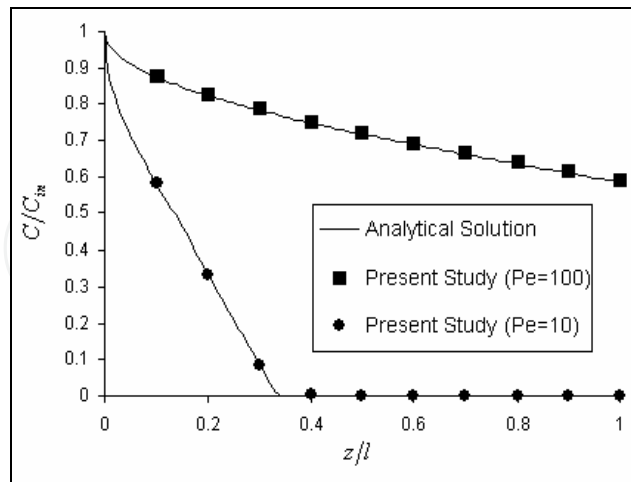

Fig. 4. Oxygen concentration at the substratum in a 2D flow cell model (Salek et al., 2007, ASME)

2.3 Shear stress and substrate concentration distribution

Figure 5(a) and (b) show the non-dimensional velocity profiles along the centerline of rectangular and square flow cells. These non-dimensional velocities are only a function of position and are independent of Reynolds number.

The shear (strain) rate contours in rectangular and square flow cells are shown in Figures 5(c) and (d) respectively. There are no secondary flows and the only shear component corresponds to the streamwise velocity. In Newtonian fluids, shear stress is proportional to shear rate ($\dot{\gamma}$) with a constant viscosity:

$$\tau_w = \mu \dot{\gamma} \tag{21}$$

The shear rate is higher at the walls where the bacteria try to attach and colonize the surface. Figure 5(e) shows the non-uniform shear stress in rectangular (aspect ratio=5) and square flow cells. In each flow cell the non-dimensional wall shear stress distribution is a function of spanwise location in the flow cell and is independent of Re. It is clear that the flow cells with higher aspect ratio can provide a uniform shear stress distribution (i.e. no spanwise shear gradient) over a large part of their surfaces. Thus, most of the bacterial biofilm formation and challenges with antimicrobials will be exposed to similar hydrodynamic conditions. Hence, results would generally be representative of the nominal (average) conditions. However, this is not true for square flow cells. Clearly the distributions differ (figure 5(e)) from each other and also from their mean (e.g. 81 for rectangular flow cell and 56 for square flow cell). For the square flow cell, significant spanwise gradients exist and there is no region of uniform shear distribution. Essentially, the nominal or mean levels are not representative of the flow conditions to which bacteria are exposed. Thus, D_h is an insufficient parameter to relate low aspect ratio flow cells. These differences in wall shear stress distribution can lead to misleading interpretation in results and may account for some of the inconsistencies observed in the literature.
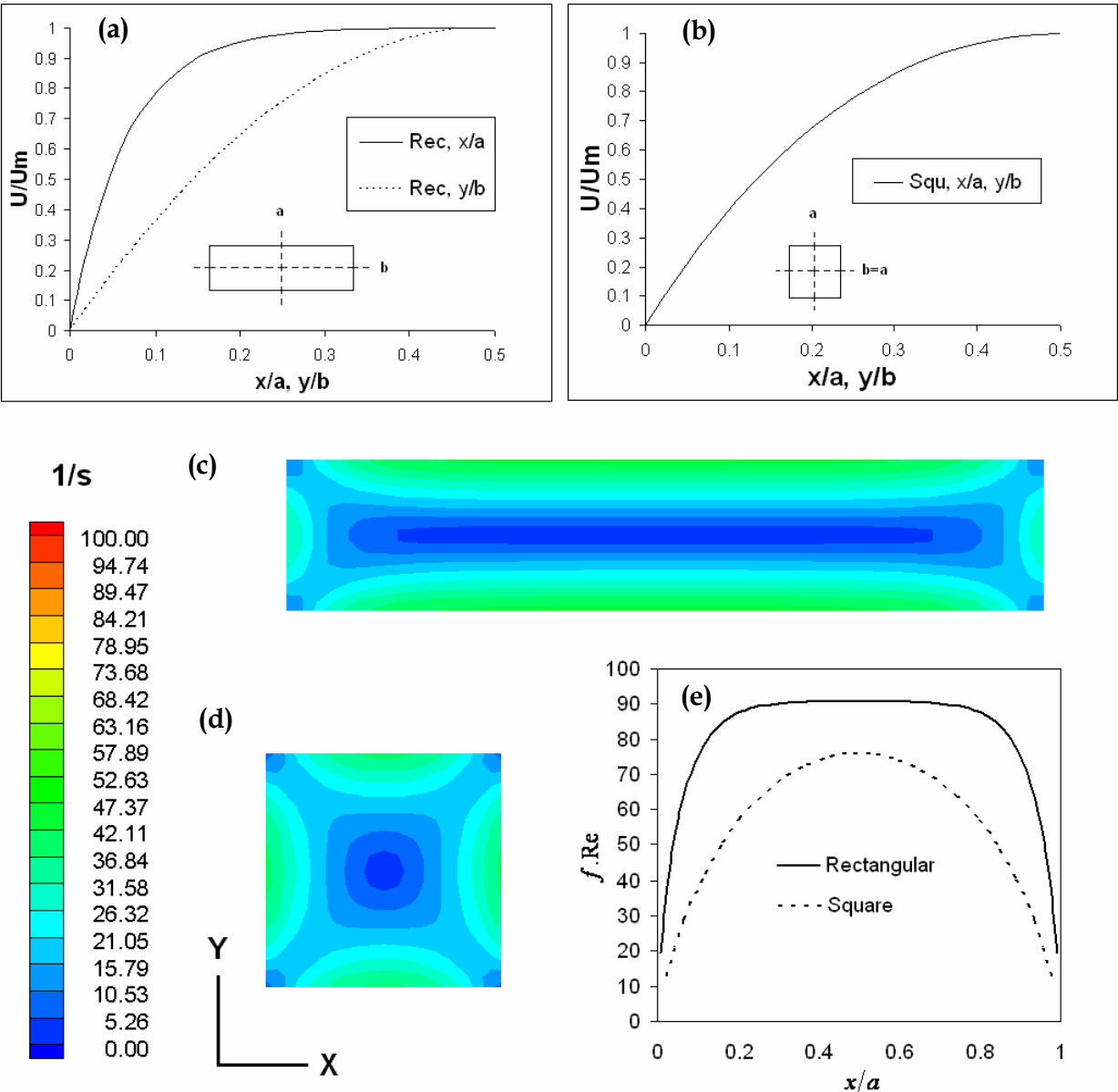
Fig. 5. Non-dimensional velocity profile along two centerlines in (a) rectangular and (b) square flow cell; Strain rate contours (1/s) (c) square tube flow cell; (d) rectangular (aspect ratio=5) tube flow cell; (e) Non-dimensional shear stress at the base of square and rectangular flow cells (Salek & Martinuzzi, 2007, ASME)

Shear plays an important role in bacterial attachment (Li et al., 1996; Thomas et al., 2002; Nejadnik et al., 2008) and biofilms morphology (Cao and Alaerts, 1995). When a cell is able to attach and resist the detachment under the shear forces, the adhesion is called stable which depends on the local fluid dynamics and the local interactions between the cell and the surface (Dickinson et al., 1995). It is been reported in the literature that in laminar flow the attachment process to the mammalian cells occurs at the shear levels between 0.25 and $0.6\,N/m^2$ (Olivier et al., 1993; Chisti, 2001); however, microbial attachment can occur at much higher shear levels (Duddridge et al., 1982). When adhered to the surfaces, bacteria can withstand higher stresses (Dickinson et al., 1995). The motile bacteria can attach more

strongly to surfaces at higher flow velocities (McClaine et al., 2002). On the other hand, it is been recently shown that the spanwise wall shear stress gradients arising in rectangular and square tube flow cells could affect the biofilm development and structure through the flow cells (Salek et al., 2009). Using the non-circular flow cells can lead to contradictory results if the presence of this spanwise shear gradient is not considered. If the non-uniform hydrodynamic condition in spanwise direction is significant, the biofilm distribution, maturity and expressed response can vary according to the location within the flow cell. In high aspect ratio flow cells, the areas with non-uniform hydrodynamics are limited to a small portion of the surfaces at the corners which makes them suitable to study the effects of shear stress level on cell adhesion and biofilm development.

Figure 6 shows the substrate concentration at different planes of a flow cell for different Peclet numbers. The distribution of substrate concentration is a function of convection, diffusion, which depends on the substrate diffusivity, and reaction rate, which depends on the biofilms characteristics. The effects of these parameters can be presented in terms of non-dimensional numbers, Pe and Da. In order to show the effects of flow cell geometry, we have isolated the other effects, and hence the biofilms characteristics and Da were assumed to be constant.

Figure 6(a) shows the substrate concentration at the base. In each cross section the substrate concentration is lower at the corners due to lower local convective mass flux. For higher Pe, the relative difference between the substrate concentration at the corner and at the middle is smaller (results not shown here). The local difference in mass concentration can cause different phenotypic biofilm responses. Picioreanu et al., (2001) numerically showed that the mushroom-like biofilm structures are due to both biofilm detachment and nutrient depletion. Both nutrient concentration and shear stress vary though each cross section which can effectively change the structure of the biofilms in different locations (Salek & Martinuzzi, 2007; Salek et al., 2009).

The present simulations can, when considering low Pe cases, explain some discrepancies seen in the literature. For example, despite of low shear stress in the corners of square channel, which reduce biofilm detachment and can increase the attachment, Ebrahimi et al., (2005) observed thicker biomass formed in the middle of honeycomb packaging channels than in the corner. They attributed these differences to local substrate limitation at the corner, and concluded that at the middle biofilms receive more nutrients. This is correct when the biofilm growth is just limited to the microbial metabolism; however, the biofilm development can be due to both increased attachment of cells and bacterial growth (Brading et al., 1995).

The substrate concentration decreases along the channel which is due to the substrate consumption by the biofilms. At lower Pe numbers this reduction is more sensible (e.g. figure 6(d)). An appropriate Pe should be chosen in long tubes to prevent substrate depletion. In fact, Pe is the ratio of convective to diffusive mass fluxes. Figure 6(b) and (c) indicates that at smaller mass Peclet numbers, the bulk concentration is influenced more by the substrate consumption at the flow cell surfaces. This is clear, because smaller Pe means weaker convective terms which can not provide enough substrate for the biofilms. In the flow with small Pe, the substrate utilization is faster than the transport of substrate, leading to greater concentration gradient through the flow cell which forms different areas of growth for the biofilms. Rich media with higher Pe, provide a more uniform environment in which the effects of nutrient availability are less pronounced. For higher Pe cases, the differences observed at the corner and middle of the flow cells should thus show more

clearly the effect of shear stresses. Inconsistencies observed in the literature can often be traced to uncontrolled variations in Pe (Salek & Martinuzzi, 2007).
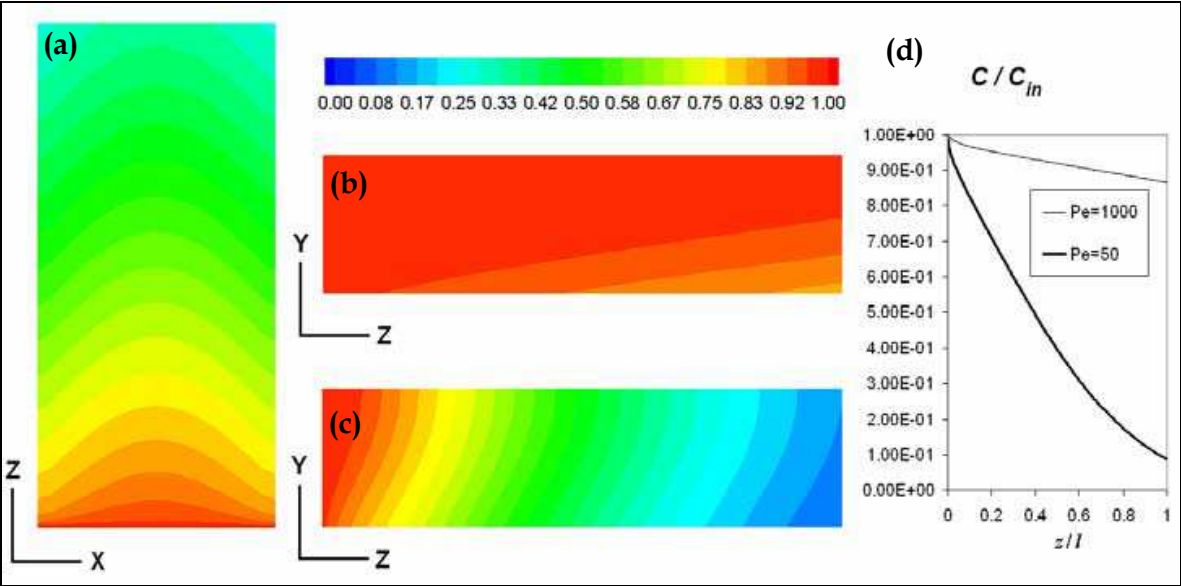

Fig. 6. Substrate concentration in the square flow cell (a) at the base at Pe=100; (b) and (C) at the mid plane at Pe= 1000 and 50 respectively; (d) at the base (Salek & Martinuzzi, 2007, ASME)

3. Unsteady flow in high-throughput 6-well plates

Devices for high-throughput assays have repeating geometric patterns, generally a well, in order to conduct many tests in parallel. When these plates are placed on an orbital shaker, the movement of the table induces the same motion in each well. The purpose of this section is to analyse the induced fluid motion in an individual well under varying acceleration conditions simulating the movement of an orbital shaker. Understanding of the fluid mechanics in these containers helps to interpret and correlate the biofilms results to hydrodynamic parameters in a well-controlled manner.

3.1 Numerical method

The unsteady two-phase flow (i.e. air and water) inside an individual well of a 6-well plate was simulated using the Computational Fluid Dynamics (CFD) code FLUENT 6.3 for different rotational speeds and volumes of fluid.

The three-dimensional unsteady Navier-Stokes and continuity equations for incompressible flow were solved in each single-phase region.

$$\frac{\partial \rho}{\partial t} + \nabla.(\rho \vec{v}) = 0 \tag{22}$$

$$\frac{\partial}{\partial t}(\rho \vec{v}) + \nabla.(\rho \vec{v}\vec{v}) = -\nabla p + \nabla(\mu \nabla \vec{v}) + \rho F \tag{23}$$

where v, ρ, μ, p and F are velocity, density, dynamic viscosity, pressure and external force (per unit mass) for the corresponding single-phase, respectively.

To capture the free surface, the volume of fluid (VOF) method was selected, in which the volume fraction of each phase in each control volume is determined. Then, based on the volume fraction of each phase, the properties (e.g. dynamic viscosity and density) of control volumes are calculated. The system of equation is then closed by solving the continuity equation for the volume fraction. Just one set of momentum equation should be solved through the domain and then the obtained velocities are shared among the phases. The geometric reconstruct scheme was employed for the calculation of transient VOF model and interface tracking. For more information please see (Salek et al., 2010a; Salek et al., 2010b).

The influence of surface tension was assumed negligible which is valid when the gravitational forces and inertial forces on the liquid phase are significantly larger than the capillary forces. These forces are expressed through the Bond and Webber non-dimensional numbers:

$$Bo = \frac{(\rho_{water} - \rho_{air})g(2R)^2}{\sigma} \tag{24}$$

$$We = \frac{\rho_{water}\Omega^2(2R)^3}{\sigma} \tag{25}$$

In the present work, Bo and We are typically of the order of 100 (i.e. Bo, We >> 1).

The orbital shaker imparts a two-dimensional, in-plane movement to the 6-well plates mounted on the table. In an orbital motion, all points undergo a circular motion horizontally with a fixed radius of gyration.

There are two methods to introduce the orbital motion numerically to an individual well (Salek et al., 2010b). While these are mathematically equivalent, the numerical implementation and the behaviour of the solution differ.

In the first method, the equations of motions are solved in a stationary frame of reference. In this case, the dynamic mesh technique is used in which the entire mesh moves with the imposed velocity by the shaker ($\vec{v} = \vec{U}$). An external C++ user defined function (UDF) linked to FLUENT was used to define the transient boundary condition for the moving well. In this method the only external force would be the gravity.

In the second method, the equations of motions are solved in a moving reference frame. In this method, the reference frame is translating with the speed of orbital shaker, and instead, the solid boundaries have zero velocity relative to the frame ($\vec{v} = 0$). The influence of the plate motion is introduced through additional momentum source terms which are the acceleration of moving reference frame, the angular acceleration effect, Coriolis and centripetal acceleration appearing in the following equation respectively:

$$\vec{F} = \vec{g} - \frac{d\vec{U}}{dt} - \frac{d\omega}{dt} \times R_p - 2\omega \times v_{rel} - \omega \times (\omega \times R_p) \tag{26}$$

In the case of orbital motion all those terms are zero except the acceleration of moving reference frame.

Both methods were implemented to verify the validity of the original assumptions. While the simulation results were in agreement within the numerical accuracy, it was found that a coarser grid and bigger time step could be used applying the dynamic mesh technique, and hence the convergence rate was much faster (Salek et al., 2010b). In moving reference frame technique, the grids and time step needed to be 2x and 6x finer respectively.

Numerical Simulation of Fluid Flow and Hydrodynamic Analysis
in Commonly Used Biomedical Devices in Biofilm Studies
207

3.2 Model verification

The motion of the free surface obtained from the CFD was compared with the captured SONY digital camera snapshots. The results were in good agreement (not shown here).

The average wall shear stress was validated experimentally using an optical shear rate (MicroS Sensor, Scientific Measurement Enterprise). The predicted shear rates agreed well with the experiments (Fig. 7(a)). The comparison of the results and the principles of sensors have been described in detail in (Salek et al., 2010a; Salek et al., 2010b).

3.3 Free surface flow and wall shear stress analysis in agitated 6-well plates

The instantaneous free-surface and wall shear stress field have been shown in figure 8. Generally, the shape of the free-surface resembles an inclined horseshoe over the elevated fluid region which undergoes a solid body rotation at the same rate as shaker's frequency. At higher frequencies, the interface is more inclined and rotates faster about the centre axis of the plate.

At 100 RPM, the fluid covers the entire bottom surface; but, in 200 RPM a small portion of the surface is exposed to the air. This can effectively change the wall shear stress magnitude due to big differences in the viscosity of air and water.

The wall shear stress at the bottom surface where the biofilms colonization occurs has been selected as the main hydrodynamic parameter here. Although the well itself does not rotate, the whole shear stress field rotates with the same frequency of the shaker. Hence the local wall shear stress at any point on the well culture area fluctuates with the same frequency of the shaker. The wall shear stress distribution is not symmetric about the center of rotation, but it is correlated with the shape of free-surface. The free surface can be characterized by a traveling wave which completes a full revolution in each period of rotation. The minimum and maximum local wall shear stress leads and lags the wave crest respectively (Salek et al., 2010b).
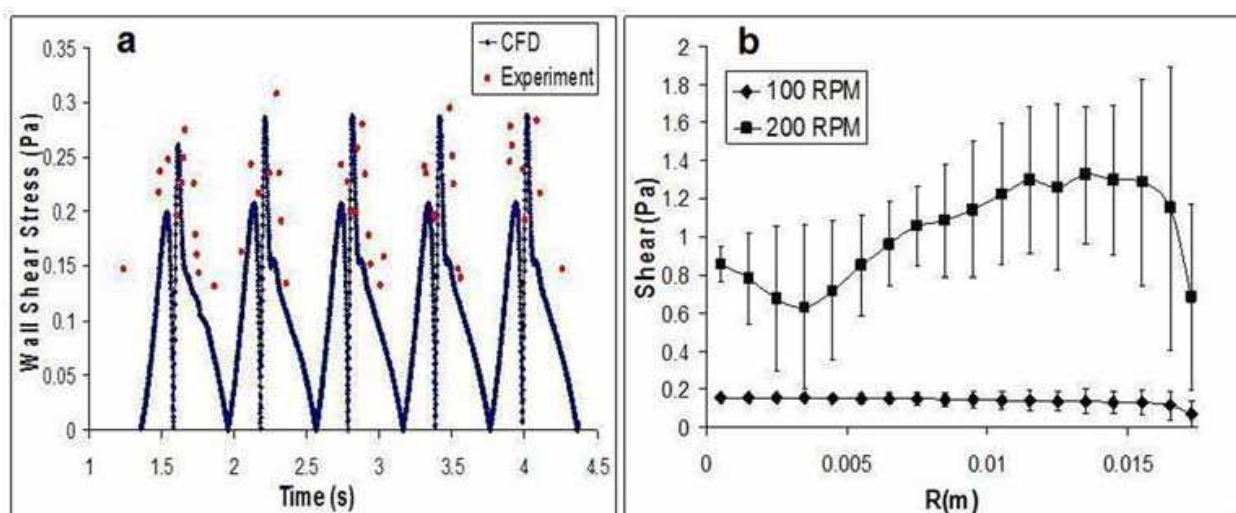

Fig. 7. (a) Time series of numerical and experimental wall shear stress component magnitude for 5 cycles at r=12mm from the center and 100 RPM; (b) Radial distribution of the mean wall shear stress magnitude at 100 and 200 RPM (Reprinted from (Salek et al., 2010a), IEEE)

Figure 7 (b) shows the radial distribution of the mean wall shear stress component magnitude (i.e time averaged at a point) at 100 and 200 RPM. It is clear that the wall shear level increases at higher rotational speeds. The shear distribution shows little variations across the plate for 100 RPM, except close to the distal corners in which the mean shear magnitude and the standard deviation of the fluctuations of the shear level magnitude are

decreased and increased respectively for both 100 and 200 RPM. This variation at the corner is due to secondary recirculation (Fig. 9) and wall effects (Salek et al., 2010b).
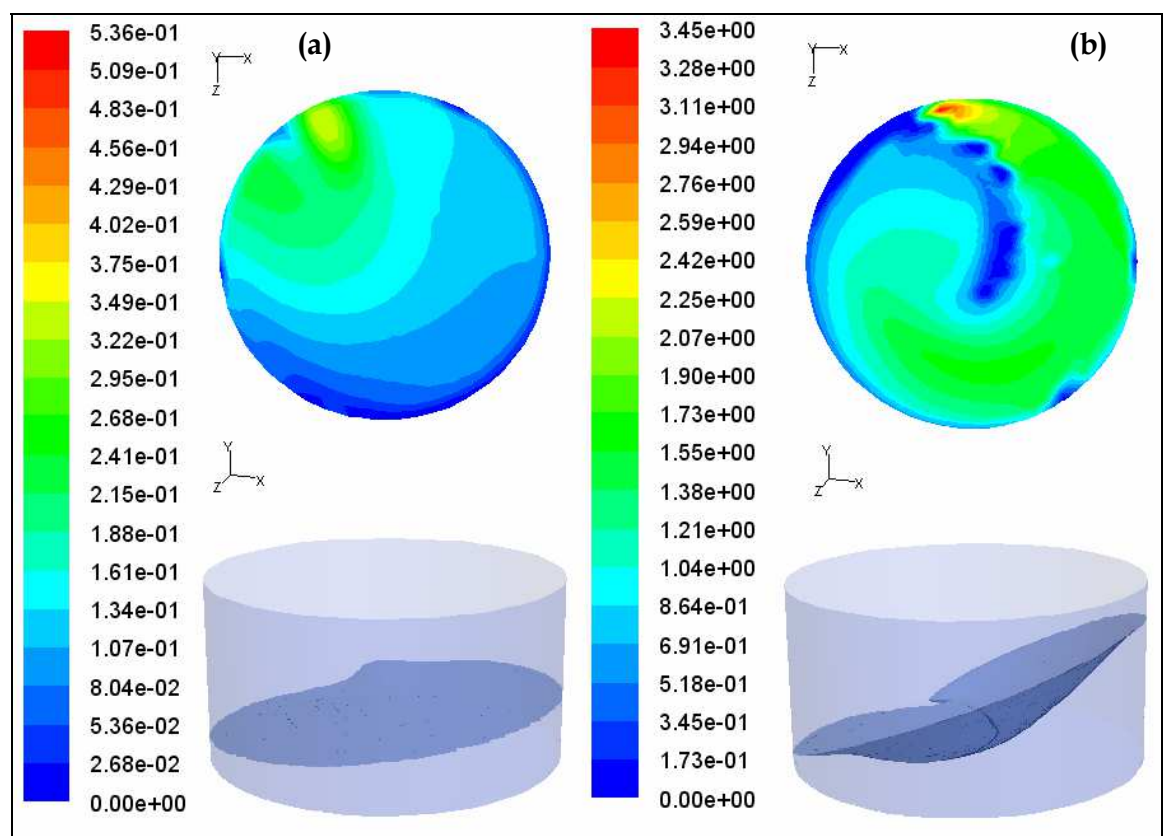

Fig. 8. Wall shear stress magnitude at the bottom wall and free-surface
(a) 100rpm, 4ml, (b) 200rpm, 4ml (Reprinted from (Salek et al., 2010a), IEEE)
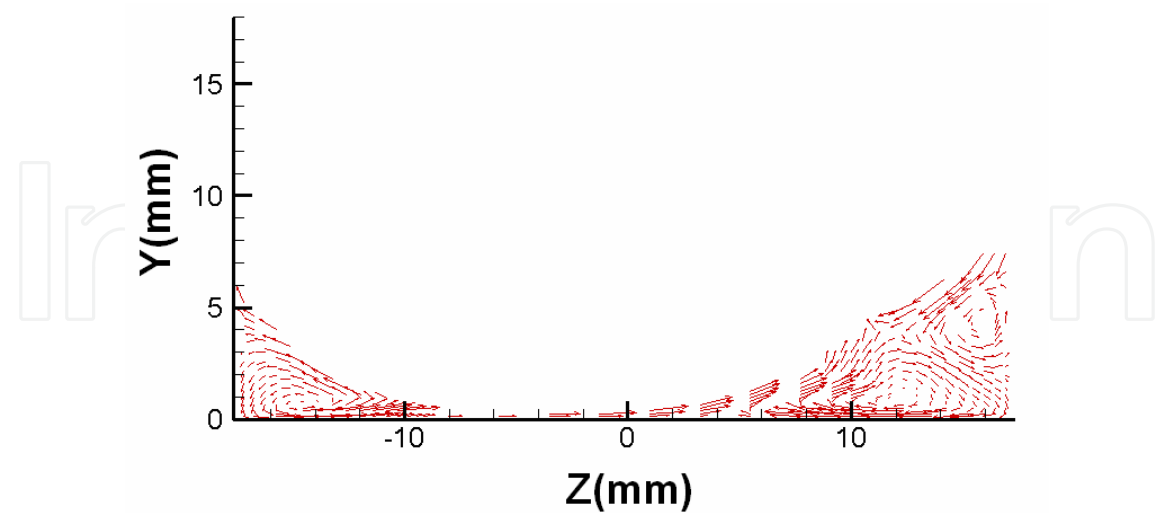

Fig. 9. Vector plots of flow in liquid phase with free-surface inside an individual well, 200rpm, 4ml

The oscillating flow behavior arising in 6-well plates can represent the physiological flows observed in vivo. Both increased shear stress levels and flow oscillation associated with plate motion were observed to contribute to biofilms formation (Kostenko et al., 2010).

4. Conclusions

In the first part of this chapter, the hydrodynamics and nutrient availability were numerically simulated inside long rectangular and square flow cells. The local substrate concentration and wall shear stress are significantly different from the mean values and are changed through the rectangular and square flow cells depending on the flow cell geometry configuration. According to the present results, high aspect ratio flow cells (e.g. parallel plate flow chambers) at higher Peclet numbers provide a more uniform environment in the flow cells.
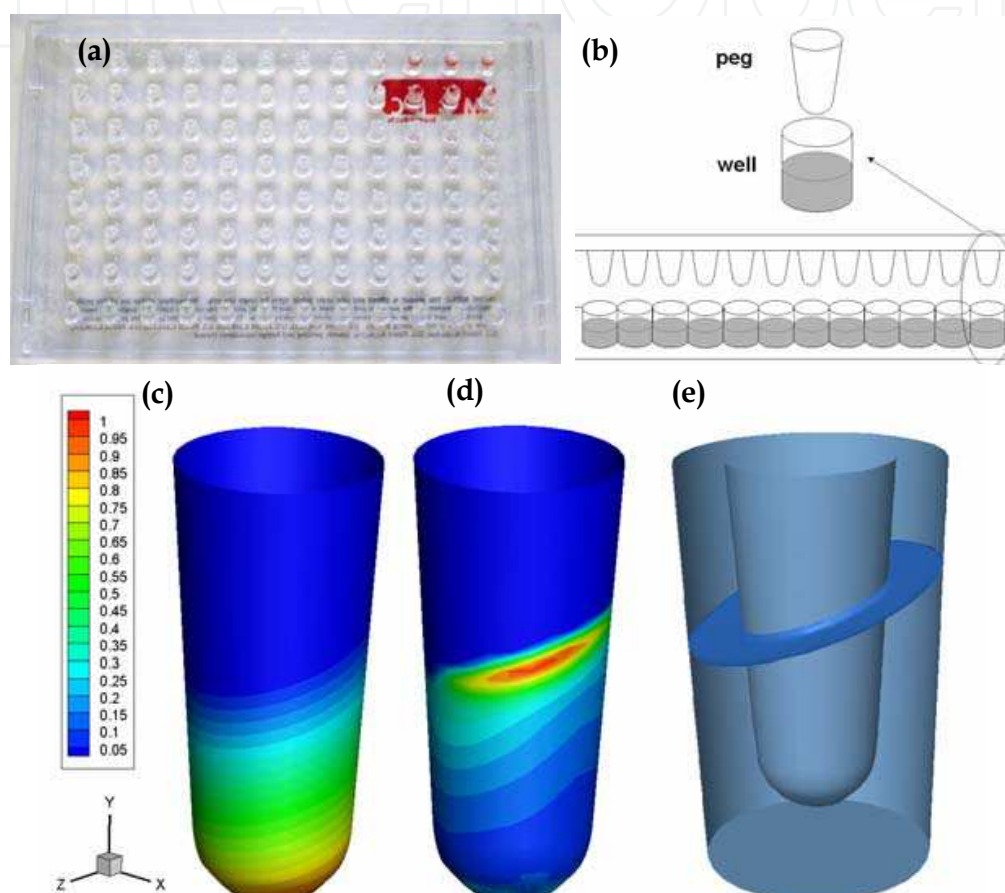
Fig. 10. (a) MBEC™ device, broadly used high-throughput device in the study of biofilms susceptibility to antibacterial agents (Ceri et al., 1999); (b) Schematic of MBEC™ device and peg and well; (c) Contours of non-dimensional static pressure over the peg; (d) Contours of non-dimensional wall shear stress over the peg; (e) Free surface flow

In the second part of this chapter, we confirmed the possibility of applying high-throughput devices to mimic physiologically relevant flow conditions to simulate the culture areas in practical applications. By controlling the hydrodynamics of the flow inside these plates, they can be more beneficial in the pathogenesis studies of biofilm infections, specially bloodstream infections.

The current methodology can be extended to other types of high-throughput devices (e.g. Fig10) as well; however, new source terms or forces may have to be considered due to the small size of some of these devices.

5. References

Brading, M.G.; Boyle, J. & Lappin-Scott, H.M. (1995) Biofilm formation in laminar flow using Pseudomonas flouorescens EX 101, *Journal of Industrial Microbiology*, 15, pp. 297-304.

Bryers, J.D. (2008) Medical Biofilms. *Biotechnol. Bioeng,* 100, pp. 1-18.

Bryers, J.D. & Ratner, B.D. (2004) Bioinspired implant materials befuddle bacteria. *ASM News,* 70, pp. 232–237.

Cao, Y.S. & Alaerts, G.J. (1995) Influence of reactor type and shear stress on aerobic biofilm morphology, population and kinetics. *Wat. Res.* 29, pp. 107-1 18.

Carslaw, H.S. & Jaeger, J.C. (1959) *Conduction of Heat in Solids*, second ed., Oxford University press, Oxford.

Castelli, P.; Caronno, R.; Ferrarese, S.; Mantovani, V.; Piffaretti, G.; Tozzi, M.; Lomazzi, C.; Rivolta, N. & Sala, A. (2006) New trends in prosthesis infection in cardiovascular surgery. *Surg Infect* 7 (Suppl 2): pp. 45–47.

Ceri, H.; Olson, M.E. ; Stremick, C.; Read, R.R.; Morck, D. & Buret. A. (1999) The calgary biofilm device: new technology for rapid determination of antibiotic susceptibilities of bacterial biofilms, *Journal of Clinical Microbiology*, 37, pp. 1771–6.

Chen, M.J.; Zhang, Z. & Bott, T.R. (2005). Effects of operating conditions on the adhesive strength of Pseudomonas flouorescense biofilms in tubes. *Colloids and surfaces. B: Biointerfaces*, 43, pp. 61-71.

Chisti, Y. (2001) Hydrodynamic Damage to Animal Cells, *Crit. Rev. Biotechnol.*, 21, 2, pp. 67–110.

Christensen, B.E. & Characklis W.G. (1989). In: *Biofilms,* Characklis, W.G., & Marshall, K.C., (Ed.), (Chapter 4), Wiley Interscience, New York, USA.

Dickinson, R. & Cooper, S. (1995) Analysis of Shear-Dependent Bacterial Adhesion Kinetics to Biomaterial Surfaces, *AIChE Journal*. 41, 9, pp. 2160-2173.

Dol, S.S.; Salek, M.M.; Viegas, K. ; Martinuzzi, R.J. & Rinker, K. (2010) Micro-PIV and CFD Studies Show Non-Uniform Wall Shear Stress Distributions Over Endothelial Cells. *Proceedings of ASME 2010, 8th International Conference on Nanochannels, Microchannels, and Minichannels*, Montreal, Canada, Aug 1-4, 2010.

Duddridge, J.E.; Kent, C.A. & Laws, J.F. (1982) Effect of surface shear stress on the attachment of Pseudomonas fluorescens to stainless steel under defined flow conditions, *Biotechnol Bioeng.,* 24, pp. 153–64.

Dunsmore, B.C.; Jacobsen, A.; Hall-Stoodley, L.; Bass, C.J.; Lappin-Scott, H.M.; Stoodley, P. (2002) The influence of fluid shear on the structural and material properties of sulphate-reducing bacterial biofilms. *J Ind Microbiol Biotechnol* 29, pp. 347–353.

Ebrahimi, S.; Picioreanu, C.; Xavier, J.B.; Kleerebezem, R.; Kreutzer, M.; Kapteijn, F.; Moulijn, J.A. & van Loosdrecht, M.C.M. (2005) Biofilm growth pattern on honeycomb monolith packings: Effect of shear rate and substrate transport limitations, *Catalysis Today,* 105, pp. 448-454.

Geesey, G.G. & Bryers J.D. (2000). Biofouling of engineered materials and systems, In: *Biofilms II: Process Analysis and Applications,* Bryers J.D., (Ed.), (237-279), Wiley-Liss, Inc., New York, USA.

Gjersing, E.L.; Codd, S.L.; Seymour, J.D. & Stewart, P.S. (2005). Magnetic Resonance Microscopy Analysis of Advective Transport in a Biofilm Reactor. *Biotechnol Bioeng,* 89, 7, pp. 822-834.

Horn, H.; Reiff, H. & Morgenroth, E. (2003) Simulation of growth and detachment in biofilm systems under defined hydrodynamic conditions, *Biotechnol. Bioeng,* 81, 5, pp. 607–617.

Hosoi, Y.; & Murakami, H., (1986). Effect of the Fluid Velocity on the Biofilm Development, *Proceedings of the Water Forum 86: World Water Issues in Evolution*, pp.1718-1725, Long Beach, California, August 1986.

Kostenko, V.; Salek, M.M. ; Sattari, P. & Martinuzzi, R.,J. (2010). Staphylococcus aureus Biofilm Formation and Susceptibility to Antibiotics in Response to Oscillatory Shear Stresses of Physiological Levels. *FEMS Immunology and Medical Microbiology*, 59, pp. 421–431.

Leutheusser, H.J. (1984) Velocity distribution and skin friction resistance in rectangular ducts, *Journal of Wind Engineering and Industrial Aerodynamics*, 16, pp. 315-327.

Li, Z.; Ho¨o¨k, M.; Patti, J.M. & Ross., J.M. (1996) The effect of shear stress on the adhesion of *Staphylococcus aureus* to collagen I, II, IV and VI. *Ann. Biomed. Eng.* 24 (Suppl. 1): S–55.

MacLeod, S.M. & Stickler, D.J. (2007) Species interactions in mixed-community crystalline biofilms on urinary catheters. *Med. Microbiol.*, 56, 11, pp. 1549-57.

Manz, B.; Volke, F.; Goll, D. & Horn H. (2003). Measuring local flow velocities and biofilm structure in biofilm systems with magnetic resonance imaging (MRI). *Biotechnol Bioeng*, 84, pp. 424-432.

Marshall, K.C. (1985) Mechanisms of bacterial adhesion at solid-water interfaces. In: *Bacterial adhesion*, Savage, D.C., Fletcher, M. (Ed.), pp. 133–161, Plenum Press, New York.

McClaine, J.W. & Ford, R.M. (2002) Characterizing the adhesion of motile and nonmotile *Escherichia coli* to a glass surface using a parallel-plate flow chamber. *Biotechnol. Bioeng.* 78, pp. 179-189.

Meda, M.S.; Lopez, A.J. & Guyot, A. (2007) Candida inferior vena cava filter infection and septic thrombophlebitis. *Br J Radiol.*, 80, 950, pp. 48-9.

Miksis, M.J. & Davis, S.H. (1994) Slip over rough and coated surfaces. *J Fluid Mech*, 273, pp. 125–139.

Murray, T.S.; Egan, M. & Kazmierczak, B.I. (2007) Pseudomonas aeruginosa chronic colonization in cystic fibrosis patients. *Curr Opin Pediatr.*, 19, 1, pp. 83-8.

Nejadnik, M.R. ; van der Mei, H.C. ; Busscher, H.J. and Norde, H. J. (2008) Determination of the shear force at the balance between bacterial attachment and detachment in weak-adherence systems, using a flow displacement chamber. *Appl. Environ. Microbiol.* 74, pp. 916-919.

Olivier, L.A. & Truskey, G.A. (1993) A Numerical Analysis of Forces Exerted by Laminar Flow on Spreading Cells in a Parallel Plate Flow Chamber Assay, *Biotechnol. Bioeng.*, 42, pp. 963–973.

Percival, S.L. & Bowler, P.G. (2004). Biofilms and their potential role in wound healing, *Wounds*, 16, 7, pp. 234-240.

Phillips, P.L.; Sampson, E.; Yang Q.; Antonelli, P. ; Progulske-Fox, A. & Schultz, G. (2008) Bacterial biofilms in wounds. *Wound Healing South Afr*, 1, pp. 10–12.

Picioreanu, C.; Van Loosdrecht, M.C.M. & Heijnen, J.J. (2001) Two-dimensional model of biofilm detachment caused by internal stress from liquid flow, *Biotechnology and Bioengineering*, 72, pp. 205–218.

Picioreanu, C.; Van Loosdrecht, M.C.M. & Heijnen, J.J. (2000) A theoretical study on the effect of surface roughness on mass transport and transformation in biofilms. *Biotechnol. Bioeng.* 68, pp. 355−369.

Presterl, E.; Lassnigg, A.; Eder, M.; Reichmann, S.; Hirschl, A.M. & Graninger, W. (2007) Effects of tigecycline, linezolid and vancomycin on biofilms of viridans streptococci isolates from patients with endocarditis. *Int J Artif Organs*, 30, 9, pp. 798-804.

Purevdorj, B.; Costerton, J.W. & Stoodley, P. (2002) Influence of hydrodynamics and cell signaling on the structure and behavior of *Pseudomonas aeruginosa* biofilms, *Appl. Environ. Microbiol.* 68, pp. 4457–4464.

Rittmann, B.E. & McCarty, P.L. (2001) *Environmental Biotechnology: Principles and Applications.* McGraw-Hill Book Co, New York.

Salek, M.M. & Martinuzzi, R.J. (2007) Numerical simulation of fluid flow and oxygen transport in the tube flow cells containing biofilms, *Proceedings of 5th Joint ASME/JSME Fluid Engineering Conference,* pp. 1-8, San Diego, USA, July 30-August 2, 2007.

Salek, M.M.; Jones, S. & Martinuzzi R.J. (2009) The influence of flow cell geometry related shear stresses on the distribution, structure and susceptibility of *Pseudomonas aeruginosa* 01 biofilms. *Biofouling,* 25, pp. 711-725.

Salek, M.M. ; Sattari, P. & Martinuzzi, R.J. (2010a) What Do Biofilms Sense in Agitated Well Plates? A Combined CFD and Experimental Study on Spatial and Temporal Wall Shear Stress Distribution, *IEEE Proc. of the 36th Annual Northeast Bioengineering Conference,* Columbia University, New York City, NY, USA, March 26-28, 2010.

Salek, M.M. ; Sattari, P. & Martinuzzi, R.J. (2010b) Numerical and Experimental Investigation of Flow and Wall Shear Stress Pattern inside Part-Filled Moving 6-well Plates, unpublished data.

Sillankorva, S.; Neubauer, P. & Azeredo, J. (2008) *Pseudomonas fluorescens* biofilms subjected to phage phiIBB-PF7A. *BMC Biotechnology*, 8 : 79.

Sousa, C.; Henriques, M.; Azeredo, J.; Teixeira, P. & Oliveira, R. (2008) *Staphylococcus epidermidis* glucose uptake in biofilm versus planktonic cells. *World J. Microbiol. Biotechnol. ,* 24, pp. 423-426.

Spiga, M. & Morini, G.L. (1994) A symmetric solution for velocity profile in laminar flow through rectangular ducts, *Int. Comm. Heat Mass Transfer,* 21, pp. 469-475.

Stoodley, P.; Dodds, I.; Boyle, J.D. & Lappin-Scott, H.M. (1999) Influence of hydrodynamics and nutrients on biofilm structure. *J Appl Microbiol,* 85 pp. 19-28.

Stoodley, P.; Jacobsen, A.; Dunsmore, B.C. ; Purevdorj, B.; Wilson, S.; Lappin-Scott, H.M. & Costerton, J.W. (2001a) The influence of fluid shear and AICI3 on the material properties of *Pseudomonas aeruginosa PAO1* and Desulfovibrio sp. EX265 biofilms, *Water Sci Technol,* 43, pp. 113–120.

Stoodley, P.; Hall-Stoodley, L. & Lappin-Scott, H.M. (2001b) Detachment, surface migration, and other dynamic behavior in bacterial biofilms revealed by digital time-lapse imaging. *Methods in Enzymology*, 337, pp. 306-319.

Thomas, W.E.; Trintchina, E.; Forero, M.; Vogel, V. and Sokurenko, E. V. (2002) Bacterial adhesion to target cells enhanced by shear force, *Cell,* 109, 7, pp. 913– 923.

Tilles, A.W.; Baskaran, H.; Roy, P.; Yarmush, M.L. & Toner, M. (2001) Effects of oxygenation and flow on the viability and function of rat hepatocytes cocultured in a microchannel flat-plate bioreactor, *Biotechnol. Bioeng.*, 73, pp. 379-389.

Trachoo, N. (2003) Biofilms and the food industry. *Songklanakarin J. Sci. Technol.*, 25, 6, pp. 807-815.

Tsanis, I.K. & Leutheusser, H.J. (1982) Non Uniform Laminar Free Surface Flow. *Journal of the Engineering Mechanics Division , ASCE*, 108, pp. 386-398.

Wenzel, R.P. (2007) Health care-associated infections: Major issues in the early years of the 21st century. *Clin Infect Dis* 45 (Suppl 1): S85–S88.

Zeng, Y.; Lee, T.S.; Yu, P.; Roy, P. & Low H.T. (2006) Mass Transport and Shear Stress in a Microchannel Bioreactor: Numerical Simulation and Dynamic Similarity, *J. Biomech Eng.* 128, 2, pp. 185-193.
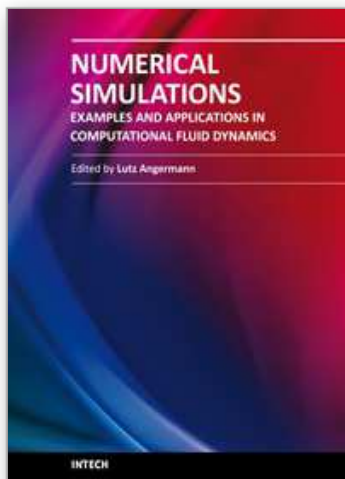
Numerical Simulations - Examples and Applications in Computational Fluid Dynamics

Edited by Prof. Lutz Angermann

This book will interest researchers, scientists, engineers and graduate students in many disciplines, who make use of mathematical modeling and computer simulation. Although it represents only a small sample of the research activity on numerical simulations, the book will certainly serve as a valuable tool for researchers interested in getting involved in this multidisciplinary ï¬eld. It will be useful to encourage further experimental and theoretical researches in the above mentioned areas of numerical simulation.

How to reference

In order to correctly reference this scholarly work, feel free to copy and paste the following:

Robert J. Martinuzzi and M. Mehdi Salek (2010). Numerical Simulation of Fluid Flow and Hydrodynamic Analysis in Commonly Used Biomedical Devices in Biofilm Studies, Numerical Simulations - Examples and Applications in Computational Fluid Dynamics, Prof. Lutz Angermann (Ed.), ISBN: 978-953-307-153-4, InTech, Available from: http://www.intechopen.com/books/numerical-simulations-examples-and-applications-in-computational-fluid-dynamics/numerical-simulation-of-fluid-flow-and-hydrodynamic-analysis-in-commonly-used-biomedical-devices-in-

INTECH
open science | open minds